

Detachable Optical Chiplet Connector for Co-Packaged Photonics

Nicholas Psaila¹, Member, IEEE, Srikant Nekkanti, David Shia, and Pooya Tadayon

Abstract—A key barrier to mainstream adoption of co-package photonics is a high-yielding and scalable assembly process. The current industry state-of-the-art for edge coupling is to attach fibers directly onto V-grooves etched into the silicon. With no ability for rework, any errors in this process will lead to loss of the entire package along with the expensive silicon committed to it. This problem is exacerbated by the yield compounding effect as the number of photonic chips on a package increases. In this article, we discuss a novel approach to overcome this limitation. Our solution relies on a glass optical bridge with integrated waveguides and connector mechanical alignment features that can be attached to the photonics silicon at die level to produce a photonics module. The bridge attach can take place using existing V-grooves or alternate registration features in the silicon for alignment. Each photonic module is then tested to ensure it is known-good prior to committing it to the package, and overall yield is no longer compounded by the number of photonic modules on the package. Other benefits of this approach are the elimination of fiber pigtailed which simplifies material handling in the manufacturing flow, and results in a fully detachable solution where the low-reliability fibers are no longer permanently attached to the expensive silicon. Low loss coupling was demonstrated using an optical bridge, with average losses from fiber into PIC of 1.41 dB. Average detachable connector losses of 0.33 dB were demonstrated along with integration into a photonic-electronic co-packaged assembly.

Index Terms—Co-packaged photonics, integrated waveguides, optical bridge, optical connector.

I. INTRODUCTION

AS TRENDS continue towards higher bandwidth and lower energy, co-packaged photonics will become a key enabler for next generation datacenters. While the concept of co-packaged photonics has been in the marketplace for many years, its adoption has been slow for a number of reasons. One reason in particular is total cost of ownership due to challenges in the assembly of such complex components [1].

The preferred optical egress in co-packaged photonic devices is through the edge. Such a scheme leaves the top surface of the device untouched and accessible for the thermal solution.

Manuscript received 19 April 2023; revised 5 June 2023 and 6 June 2023; accepted 8 June 2023. Date of publication 12 June 2023; date of current version 2 October 2023. (Corresponding author: Nicholas Psaila.)

Nicholas Psaila is with the Intel Corporation, EH54 7EJ Livingston, U.K. (e-mail: nicholas.psaila@intel.com).

Srikant Nekkanti is with the Intel Corporation, Chandler, AZ 85226-3699 USA (e-mail: srikant.nekkanti@intel.com).

David Shia and Pooya Tadayon are with the Intel Corporation, Hillsboro, OR 97124-6497 USA (e-mail: david.shia@intel.com; pooya.tadayon@intel.com).

Color versions of one or more figures in this article are available at <https://doi.org/10.1109/JLT.2023.3285149>.

Digital Object Identifier 10.1109/JLT.2023.3285149

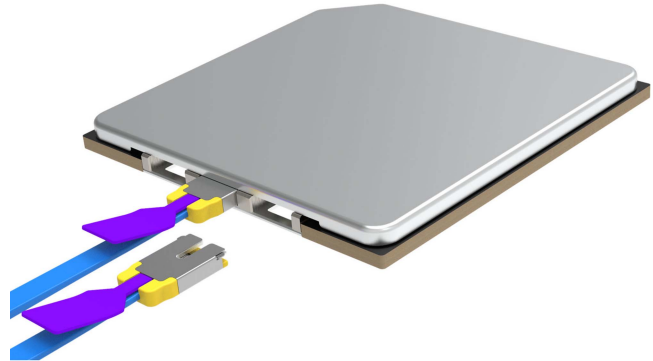


Fig. 1. Illustration of an ideal detachable on-package optical connector.

The industry state-of-the-art for edge coupling is to attach fibers directly to the photonic IC (PIC) with the aid of V-grooves etched into the silicon which provide a mechanical registration feature to align the fibers to the waveguides in the silicon [2]. In today's assembly process, these fibers are attached at the last step, after all the expensive silicon components have been committed to the package substrate. As a result, any errors or mistakes in the fiber attach process will render the entire assembly a loss as there is no rework opportunity. The problem is exacerbated by constructions where multiple PICs go onto the same package and the resulting yield is compounded by the incorporation of each additional PIC.

Aside from the yield challenge stated above, there are practical scalability challenges with this approach. For example, the dangling fibers challenge the downstream material handling systems that the parts need to go through for end-of-line assembly and test operations. These fibers present similar handling challenges at the customer, and due to the lack of a re-work process, a failing fiber in the customer environment will lead to scrapping the entire unit.

An ideal solution is one in which the optical attach process can take place at the wafer/die level with a subsequent test step that ensures the attach was done correctly prior to committing the photonic IC to the package. Furthermore, the ideal solution would also eliminate the dangling fibers and allow the fiber-array-unit (FAU) to be plugged directly into the device by the customer, similar to a universal serial bus (USB) connector. Fig. 1 below shows an ideal detachable on-package optical connector topology.

Many solutions have been proposed to tackle the challenges highlighted above, each with their own limitations and barriers to

implementation [3], [4], [5], [6]. At Intel, we've chosen to pursue an optical bridge strategy based on integrated 3D waveguides in a glass structure that allow for the optical attach to take place at the beginning of the assembly process and enable a fully detachable solution in the field. In this article, we will describe the bridge manufacturing process along with how it is attached to the PIC and tested. Also covered in this article is an overview of the custom pluggable FAU which interfaces with the optical bridge. Finally, we will discuss future architectures and constructions that can be enabled by these core building blocks.

II. OPTICAL BRIDGE DESIGN AND MANUFACTURING

A. Glass Bridge Manufacturing Technologies

Glass has been used for optical waveguiding applications for several decades, with a variety of manufacturing approaches available to process glass materials into optical waveguides. These include well established techniques such as ion-exchange, flame hydrolysis deposition, chemical vapor deposition and direct laser writing [7], [8], [9]. Glass can offer inherent material properties that makes it well suited for photonic integration in co-packaging applications, such as low optical losses, mechanical stability, a co-efficient of thermal expansion which can be close or equal to that of silicon, and resilience to the thermal cycles typically seen during semiconductor assembly processing.

The glass bridge devices used in this work were manufactured using ultrashort-pulse laser direct writing, which enables wafer-scale single-step 3D patterning of waveguides and precise micromachined features [9], [10], [11], [12]. This technique has the unique advantage of allowing 3D routing of waveguide circuits to provide robust interconnection between large arrays of inputs and outputs. This enables features such as channel pitch conversions and height transitions within the bulk glass, which can have substantial advantages in aiding geometrical packaging constraints, and opens up the third dimension to increase channel density when interfaced with two-dimensional fiber array units. The waveguide propagation loss is typically in the region of 0.2 dB/cm [13], [14].

In recent years, ultrashort pulse laser direct writing has developed into a high throughput industrial manufacturing process, capable of high volume production [15]. Process throughput and unit costs are competitive and there is line-of-sight to drive further improvements.

Fig. 2 shows an example glass optical bridge which is configured to interface in an edge coupled configuration to a PIC. The waveguides fan out from a 1x16 configuration and remap into a 2x8 channel array for connection to a 2x8 fiber connector.

In addition to the waveguides, the optical bridges can also contain precise 3D laser micromachined structures which can be processed in the same patterning step as the waveguides, thus minimizing registration errors between waveguides and mechanical features that allow for passive mating to optical fiber connectors. On the opposing side, the bridge can contain mechanical features to allow registration and passive mating to corresponding mechanical alignment features on the PIC. A wide range of alignment structures are possible, including structures designed to interface to fibers such as V-grooves,

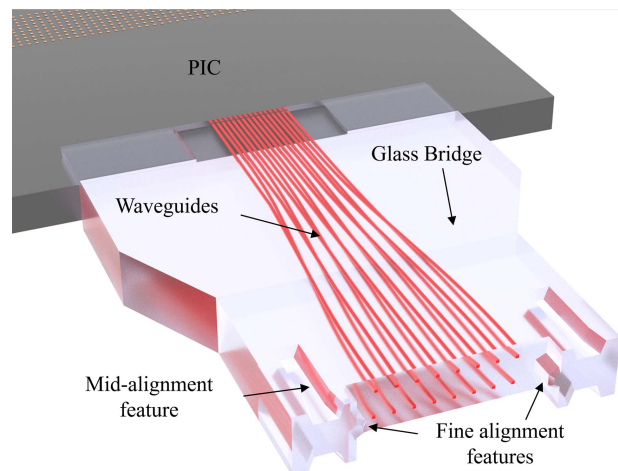


Fig. 2. Example optical bridge containing 3D routing waveguides and embedded connector alignment features.

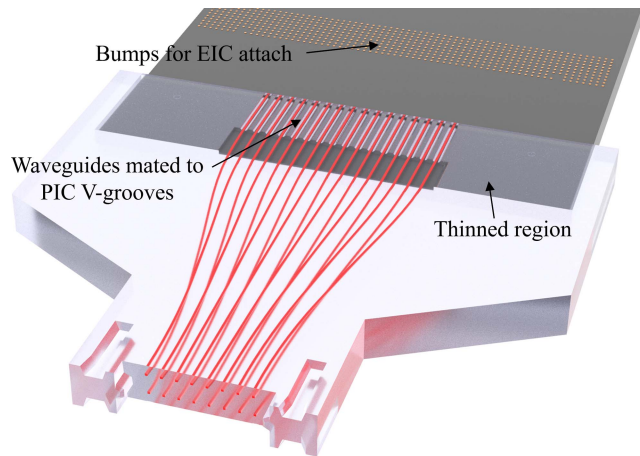


Fig. 3. Optical bridge containing 3D waveguides, connector alignment features, and PIC mating features.

or structures shaped appropriately to fit to existing mechanical alignment structures on PICs such as trenches or grooves.

B. Optical Bridge Design and Configuration

The optical bridge used in this work is designed to interface to a pre-existing silicon photonic integrated circuit containing embedded V-grooves, which are fabricated using wet etching to create angled planes along the (111) crystallographic plane of the silicon substrate. The V-grooves in this case are designed to interface to a conventional 250 μm pitch optical fiber ribbon, however substantially smaller channel pitches of <30 μm are possible, particularly if a co-design between the PIC and glass bridge is carried out.

At the connector side of the bridge, 3D micromachined features are present to allow for mechanical mating of a corresponding glass connector ferrule, which contains opposing mating features. The design of the connector is described in Section III.

Fig. 3 shows an example of an optical bridge designed to passively align to a PIC containing embedded V-grooves. At the

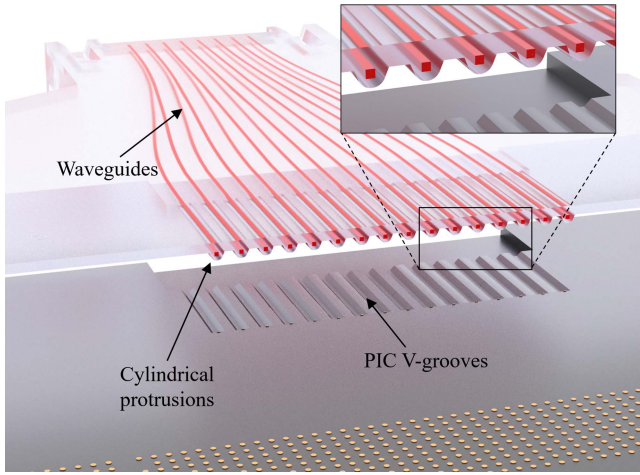


Fig. 4. Close-up of the bridge to PIC interface. The two bodies are separated for illustration purposes (waveguides not to scale).

PIC interface side, the glass bridge is wider than the PIC which allows for regions of increased glass thickness on either side, aiding mechanical rigidity.

Fig. 4 shows a close-up view of the interface between the optical bridge and the PIC V-grooves with the two interfaces separated for illustration purposes. Cylindrical protrusions are present on the glass bridge with the laser written waveguides positioned at the center point of the cylinder which allows the structure to mimic an array of optical fibers. This allows for passive assembly onto a PIC containing existing V-grooves optimized for optical fibers.

A Monte Carlo analysis was carried out in order to assess the predicted optical insertion losses of the bridge to PIC assembly, taking into account the mechanical alignment tolerances, mode field diameters, and on chip losses of the PIC and optical bridge. A loopback optical coupling model was used with a bridge to PIC alignment tolerance (3σ) of $1.58 \mu\text{m}$, using a glass waveguide mode field diameter at the PIC interface of $6.5 \mu\text{m}$. Fig. 5 below shows the results of the Monte Carlo analysis.

Based on the tolerance stack up, the predicted insertion loss distribution for a full loop fiber-bridge-PIC-bridge-fiber loop-back peaks at 5.2 dB , including approximately 3 dB of PIC mode conversion and on-chip losses. This corresponds to a 1.1 dB loss for single-pass transmission from the PIC and into the fiber.

III. OPTICAL BRIDGE FABRICATION AND TEST

Sixteen channel optical bridges were fabricated on 150 mm glass wafers, which were designed to interface to a silicon PIC containing passive alignment V-grooves and loop-back waveguides for optical test purposes.

The cylindrical protrusions manufactured on the glass bridge were designed to mimic optical fibers, having a radius of curvature of $62.5 \mu\text{m}$. Protrusions sampled from 48 die across 4 wafers were profiled using white light interferometry. Cylindrical fits were applied, allowing automated measurement of the radius of curvature of the cylinder across the set of structures. Fig. 6 below

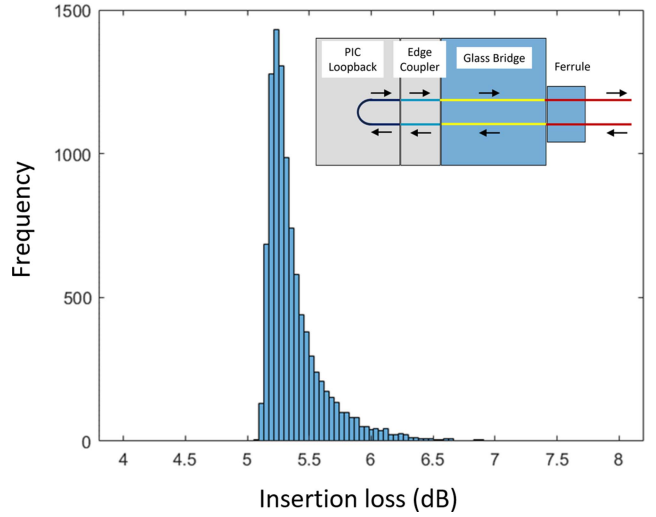


Fig. 5. Monte Carlo analysis of loopback losses of optical bridge and PIC.

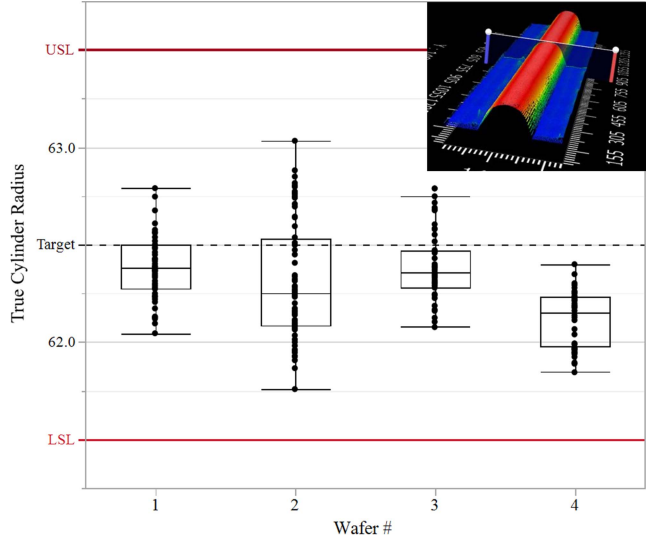


Fig. 6. Measured radii of curvature for cylindrical mating features on the glass bridge. Inset shows a 3D plot of the surface profilometry data for a single cylindrical protrusion.

shows the measured data. The measurement error was assessed by 30 repeated measurements of the same 16 channel die, resulting in a worst-case 3σ measurement error of $\pm 0.084 \mu\text{m}$.

The measured data shows mating feature radii of curvatures which are well within the design envelope tolerances defined by the USL and LSL levels. The mechanical tolerances observed are within the equivalent $\pm 0.8 \mu\text{m}$ radial position tolerance limits for standard single mode optical fibers, when diameter and core-cladding concentricity tolerances are combined [16].

The optical bridges were assembled passively to the PIC V-grooves using vision-based pre-alignment followed by mechanically inserting the glass bridge into the PIC V-grooves. UV cured index matching epoxy was used to permanently attached the glass to the PIC. The epoxy used has a linear shrinkage specification of 1.5%, however due to the passive mechanical

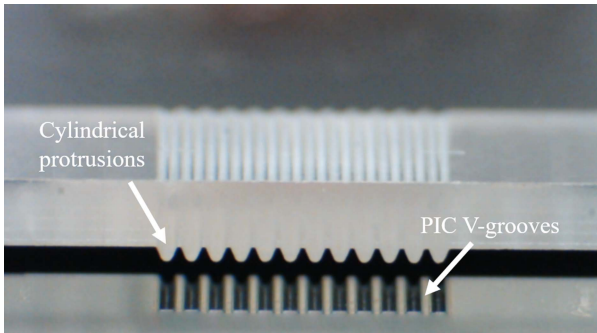


Fig. 7. Microscope image of glass cylindrical protrusions and PIC V-grooves during assembly process.

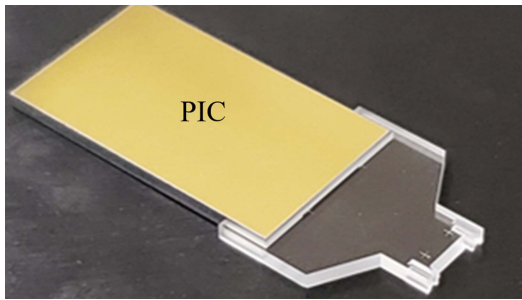


Fig. 8. Optical bridge and PIC forming a fully testable optical sub-assembly.

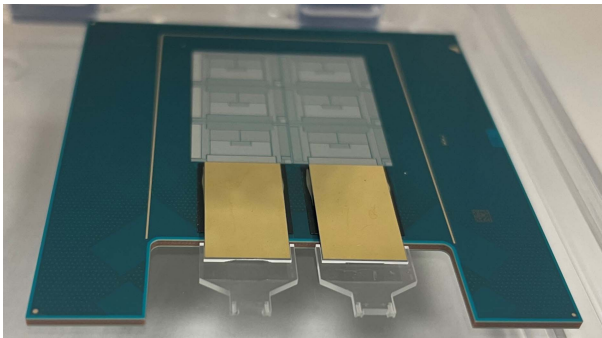


Fig. 9. Organic package containing two optical sub-assemblies.

registration of the bridge to the PIC, the impact of epoxy shrinkage on the performance of the optical bridge is not a concern. Fig. 7 shows a microscope image of a 12-channel glass bridge being assembled to a 12-channel test PIC.

The assembled PIC and bridge then form an optical chiplet sub-assembly module which can be fully electrically and optically tested to generate a known-good photonic module prior to committing it to the final package. Fig. 8 below shows a PIC and bridge subassembly, and Fig. 9 shows a pair of sub-assemblies attached to an organic substrate. The optical bridges used in this example were approximately 8.6 mm in length, 10 mm in width, and 0.8 mm in height.

For the sub-assemblies used in this work, passive loopback PICs were used for optical characterization, therefore in this case only a passive optical test was carried out.

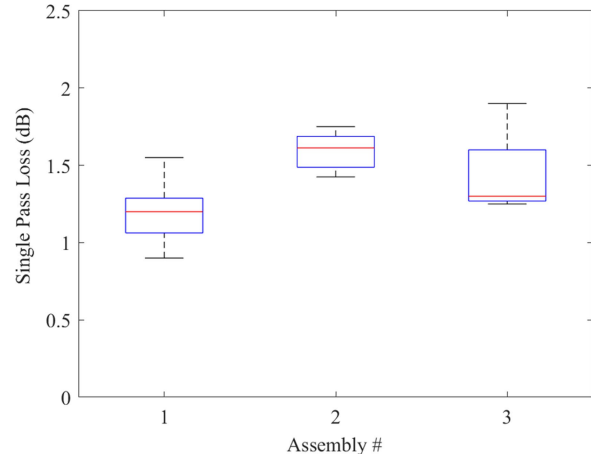


Fig. 10. Single-pass (FAU-bridge-PIC) losses for three separate assemblies.

Three assemblies containing optical bridges assembled to PICs were tested for optical insertion loss at a wavelength of 1310 nm, with 8 full loopbacks per assembly. Reference power measurements were taken at the input launch fibers and do not include the fiber-to-fiber connectors. The approximate PIC on-chip losses (including spot size converters) of 3 dB were subtracted from the loopback losses to allow for calculation of the single-pass loss. Fig. 10 below shows the single pass loss for the three assemblies.

The measurements of the three assemblies show average single pass losses of the PIC to bridge to fiber coupling of 1.19, 1.59 and 1.45 dB, which is in good agreement with the 1.1 dB loss predicted by the Monte Carlo analysis cited above. Due to the loopback testing configuration, a detailed breakdown of the loss contributions is not possible, however from simulations of the optical coupling we estimate approximately 0.4 dB originates from the bridge to PIC interface and 0.6 dB from Fiber to bridge interface including Fresnel losses. The loss variation is primarily attributed to mechanical variability in the PIC to bridge optical interface, as well as variations in the PIC spot size converter losses. Loss reductions are possible through adjustments to the assembly process, mode field matching, antireflection coatings at the connector interface, and design modifications to reduce the points of contact and contact variability on both PIC and glass-bridge mechanical features. Reducing the points of contact offers a route to improve loss variability by reducing the amount of area of the PIC and bridge to be kept free of defects and particulate contamination.

IV. FAU CONNECTOR DESIGN

The proprietary low-profile blind-mate connector described in this section is custom designed for co-packaged photonic applications and contains multiple cascading stages of mechanical alignment, finishing with a tightly tolerated CTE-matched glass to glass mating to the optical bridge.

Fig. 11 shows an overview of the key elements that constitute the pluggable and detachable connector FAU assembly. This includes:

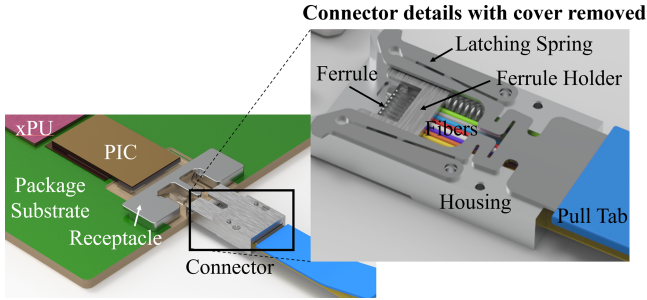


Fig. 11. Overview of the key elements that constitute the blind-mate detachable connector design.

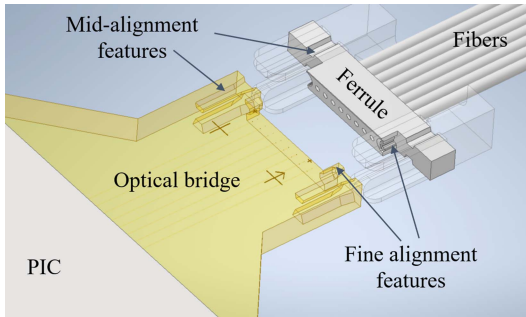


Fig. 12. FAU Connector ferrule with inserted fibers and various alignment features.

- 1) Glass connector ferrule consisting of through holes to house the fibers, and alignment features to mate with optical bridge.
- 2) Ferrule holder to guide the multi-stage alignment.
- 3) Connector latching spring mechanism assembly responsible for retainment to the PIC-package and to enable connector insertion and detachment.
- 4) Connector housing to contain all the connector elements.
- 5) Receptacle attached to the PIC package to engage the connector latching spring and provide coarse alignment with the housing.

The glass ferrule consists of a single micromachined glass piece with precise through holes for fibers to be inserted, bonded and polished. The ferrule also consists of 3D laser micromachined mechanical features for passive alignment and mating with the opposing features in the optical bridge, as described in Section II.

The ferrules are manufactured at a wafer scale using the direct laser writing methods described in Section II. Using ultrashort pulse direct laser writing in glass enables single step patterning of complex 3D mechanical features combined with fiber alignment holes, and can scale to large channel counts with diameter and position tolerances well below $\pm 0.5 \mu\text{m}$. Fig. 12 shows an example of an 8-channel ferrule containing fibers and both mid and fine alignment features. The dimensions of the ferrule in this example are 4 mm in width, 1.1 mm in length and 0.8 mm in height.

The final alignment between the fibers in the ferrule and the waveguides in the optical bridge is based on a multi-stage

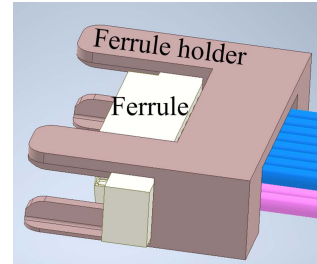


Fig. 13. Ferrule holder assembled to ferrule.

alignment process. A ferrule-holder is assembled onto the connector ferrule, and enables a middle-stage alignment between the optical bridge and the ferrule. The lead-in edge of the holder engages and slides onto the coarse alignment features of the optical bridge when the connector is pushed forwards during the mating process. Fig. 13 shows a schematic of the ferrule and ferrule-holder.

The final-stage alignment between the fibers in the ferrule and the optical waveguides is reached when the fine alignment features in the ferrule and the optical bridge mate with each other. The multi-stage alignment process is illustrated in Fig. 14.

The final glass-to-glass mating interface is an air-gap based design with a nominal gap size of $10 \mu\text{m}$, with both facets angled at 8 degrees to minimize back-reflections. The use of an air-gap based design allows for reduced mating forces and a relaxed angular tolerance for the ferrule polished facet, as the angular tolerance requirements would be particularly tight in order to achieve physical contact in a rigid glass-to-glass mating scheme. Beam refraction is taken into account by pre-compensating the position of the optical waveguides, and the losses due to Fresnel reflections can be mitigated by antireflection coating of the two surfaces. In this work no AR coatings were used at the glass-air interfaces, resulting in approximately 0.3 dB of reflection loss per pass.

Additional springs in the connector housing, as shown in Fig. 15, limit the contact force between the ferrule and the optical bridge and allow for lateral float of the ferrule and holder within the housing. The mating alignment features in the optical bridge and ferrule need to be designed with appropriate tolerances to ensure precise alignment with the fiber and the bridge waveguides.

A Monte Carlo analysis was carried out to assess the predicted alignment with the fibers and the optical bridge waveguides taking mechanical fabrication and assembly tolerances into account, the results of which are shown in Fig. 16. 3σ alignment tolerances of $\pm 0.25 \mu\text{m}$ were used for the ferrule fine-alignment features and $\pm 0.5 \mu\text{m}$ for the bridge fine-alignment features.

The 3σ alignment tolerances of $0.62 \mu\text{m}$ compare favorably to those shown for fiber to V-groove alignment in [2], where the 3σ alignment tolerance was shown to be approximately $1.3 \mu\text{m}$.

While the alignment features in the connector ferrule and the optical bridge are important to ensure optical performance of the connector, equally important are the retention design features to ensure connector retention to the package. To this effect, latching features were added to the connector design.

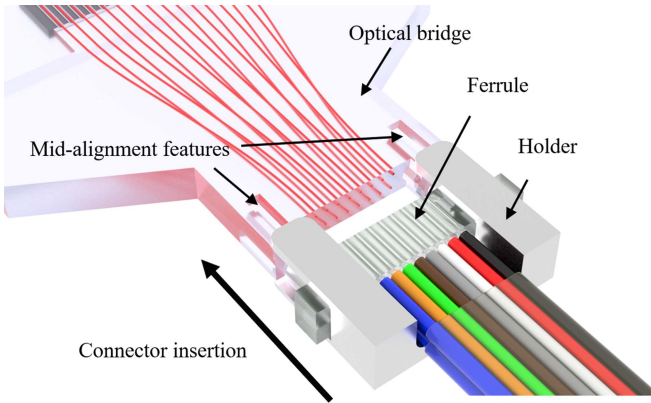
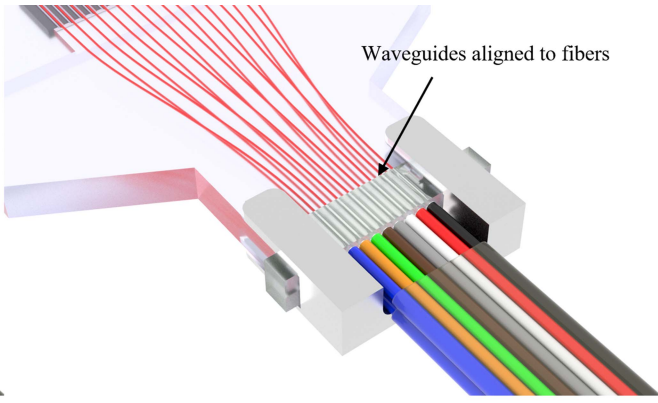
**1st stage of alignment between bridge and ferrule****Final stage of alignment**

Fig. 14. Staged mating between FAU connector ferrule and optical bridge. Left shows the ferrule holder engaging with the mid-alignment features, Right shows the final glass-to-glass mating of the fine alignment features on ferrule and bridge.

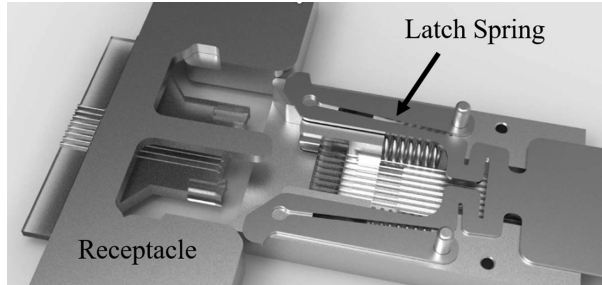
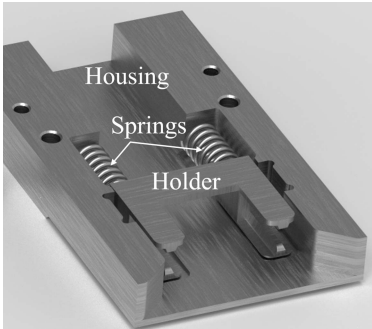


Fig. 15. Springs in the FAU connector housing limit contact force between ferrule and optical bridge. Note: Not all connector components are shown for clarity of illustration.

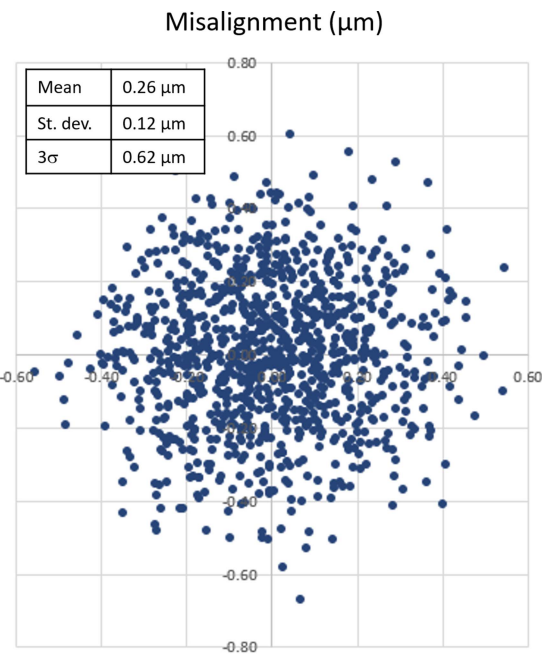


Fig. 16. Monte Carlo simulation results showing alignment tolerance <0.7 μm .

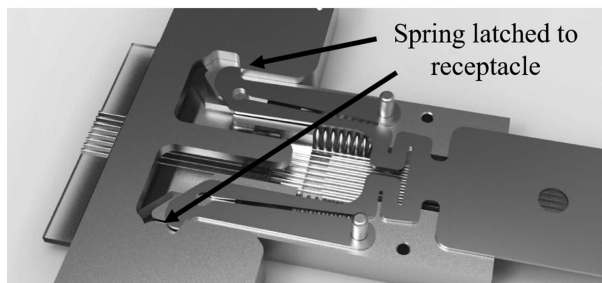
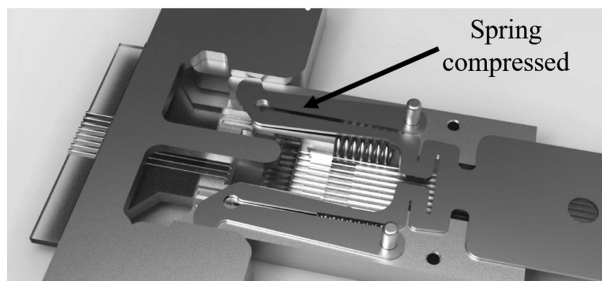


Fig. 17. 3D render of connector latching mechanism.

The latching spring mechanism was designed such that when the connector is pushed towards the PIC package, the spring latches are pushed inwards and then release and engage with the receptacle retention features as shown in Fig. 17.

The retention latch springs were integrated to a connector pull tab for optimal user experience so that a user can grab

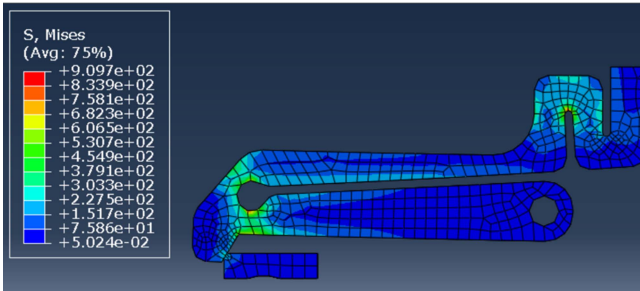


Fig. 18. Latch spring stress simulation. Maximum stress is ~ 910 MPa.

the pull tab, push the connector to plug to the PIC package and also pull on the tab to release the latch springs from the receptacle thus detaching the connector. Therefore, the design of the connector retention and package receptacle features enable a pluggable and detachable blind-mate FAU connector.

Finite element simulations were carried out on the latching spring to study the mechanical stresses in the spring and the results are shown in Fig. 18. While the latching design can be further optimized, the results indicate that high strength steel with yield stress ~ 1000 MPa would be a suitable material candidate to ensure no permanent deformation and the survival of multiple insertion-detach cycles.

Based on the spring rate of the two coil springs and the designed over-travel, the mating force between the connector and the glass bridge has been estimated to be approximately 1.5 N. For reference, a typical USB type C connector requires 5–20 N insertion force to ensure stable electrical connections between connector pins and mating printed circuit board (PCB) pad [17]. To determine the resultant shear stress that develops at the interface between the coupler and the PIC, it is assumed that a minimum bonding area of 1.0 mm^2 exists. This combination gives rise to a shear stress magnitude of $1.5\text{ N}/1.0\text{ mm}^2 = 1.5$ MPa. Given that most adhesives have a shear strength greater than 10 MPa, the risk of connector damaging the coupler-to-PIC interface is low. The risk is further reduced when the bonding area is increased beyond the initial assumption of 1.0 mm^2 .

V. DETACHABLE CONNECTOR MANUFACTURING AND TEST

Prior to assembly, geometrical measurements of the critical ferrule dimensions were carried out. The pitches between fiber positioning holes in the glass ferrules were measured using a high precision optical Co-ordinate Measurement Machine (CMM). Fig. 19 below shows hole pitch values measured over several ferrules, showing 3σ tolerances of $\pm 0.245\text{ }\mu\text{m}$. This compares favorably to the typical feature-to-feature mechanical alignment tolerances achieved in ‘Elite’ grade MT ferrules, with 6σ values quoted as $\pm 2\text{ }\mu\text{m}$ [18].

Eight channel single mode fiber ribbons were assembled into the glass ferrules and were then optically polished to an 8 degree facet angle. The ferrules were assembled into the ferrule holders and then into the connector housings as described in Section III. The receptacle with retention features was bonded to the integrated heat spreader of the package, and allows for coarse connector alignment and latching of the spring loaded

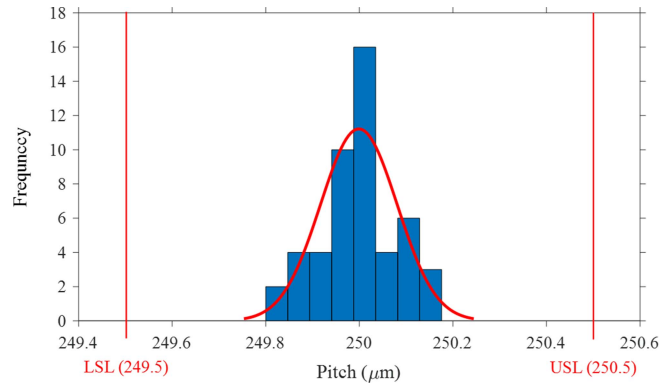


Fig. 19. Hole-to-hole pitch measurements of glass connector ferrules taken using an optical CMM tool.

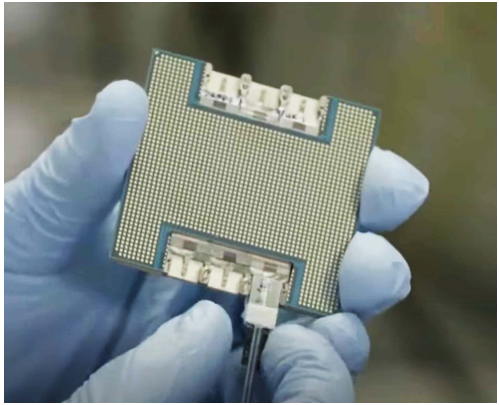


Fig. 20. Co-packaged photonic assembly with six detachable optical interfaces.

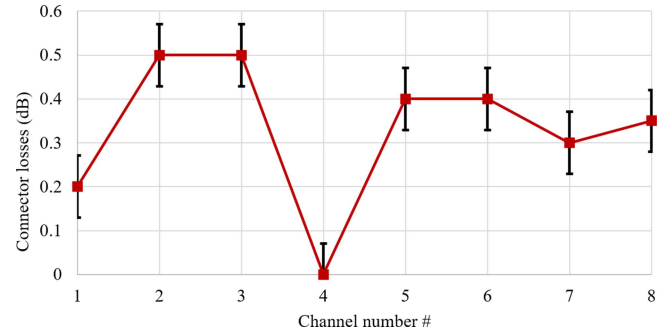


Fig. 21. Connector losses for an 8-channel detachable connection to an optical bridge. Measurement resolution is 0.05 dB .

connector. Fig. 20 below shows a photograph of an example co-packaged assembly with 6 detachable optical interfaces.

The first prototype detachable optical connectors were tested using an 8-channel optical bridge, using an 8 channel connector ferrule in a 1×8 configuration with $250\text{ }\mu\text{m}$ pitch. Fig. 21 below shows the optical connector losses, which were measured by taking the difference between the passively mated insertion loss and a separate measurement where each channel is actively aligned individually without the connector ferrule. This provides a measure of the loss penalty from misalignment when plugging in the detachable connector.

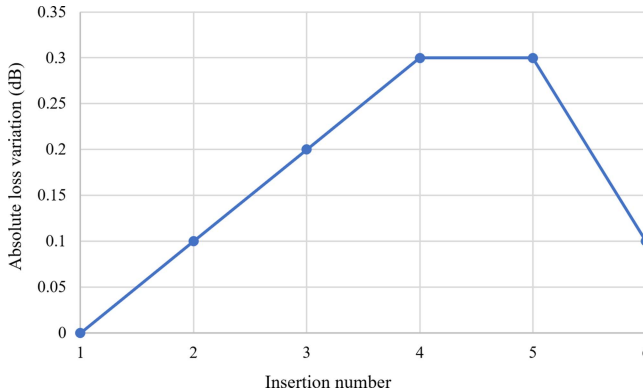


Fig. 22. Absolute loss variation for repeated insertions.

Average connector losses of 0.33 dB were observed with channel 4 showing a well aligned channel, achieving within 0.07 dB of the active alignment value. The connector losses can be primarily attributed to mechanical alignment of the fibers and ferrule mating in the prototype connector. Future work will focus on refinement of the fiber assembly and connector alignment features.

Preliminary repeated insertions of the connector to glass bridge coupling were carried out, as shown in Fig. 22 below.

A total of 6 repeated insertions were carried out on the prototype connector, with an average absolute loss variation of 0.17 dB. A wider study on the repeatability of connector insertions will be presented in future work. We attribute the loss variation primarily to the connector mating mechanics, with further refinement of the connector expected to yield substantial improvements in loss repeatability.

VI. FUTURE ARCHITECTURES

The configurations described in the previous sections focus on edge coupling to PICs, however the optical bridge technology can be extended to a wide range of coupling configurations, including broadband adiabatic coupling [19], [20], and vertical coupling geometries. High quality micro-optic elements can be integrated into the glass platform alongside the waveguides and micromachined optical elements to form collimating or focusing optics, enabling applications such as expanded beam formation. Curved micromirrors can be formed in arrays allowing for low loss light-turn coupling to PICs or connectors containing corresponding vertical coupler elements.

The technology described in the previous sections can also be further integrated into high density photonic-electronic interposers containing through-glass-vias and multi-layer electrical redistribution layers for glass-based package substrates [8].

VII. CONCLUSION

In conclusion, this article describes a detachable optical bridge and connector architecture suitable for high volume production in co-packaged photonics applications. The architecture enables known-good optical attaches to be assembled in chiplet sub-assembly format and several key building blocks have been demonstrated. Optical bridges containing 3D waveguides and

connector alignment features were passively aligned to PICs containing embedded V-groove features. A custom detachable connector was demonstrated allowing pluggability directly into the package. Average connector losses of 0.33 dB were demonstrated along with integration into an existing photonic-electronic co-packaged assembly.

ACKNOWLEDGMENT

The authors would like to acknowledge John Macdonald, Stewart Barrows, Debaditya Choudhury, Duncan Dore, Eric Moret, Jonas Croissant, Xavier Brun, Mohanraj Prabhugoud, and Wesley Morgan for assistance with the design, fabrication, and characterization of the optical bridge and connector.

REFERENCES

- [1] N. Margalit et al., "Perspective on the future of silicon photonics and electronics," *Appl. Phys. Lett.*, vol. 118, 2021, Art. no. 220501.
- [2] T. Barwickz et al., "Automated, high-throughput photonic packaging," *Opt. Fiber Technol.*, vol. 44, pp. 24–35, 2018.
- [3] C. Scarella et al., "Pluggable single-mode fiber-array-to-PIC coupling using micro-lenses," *IEEE Photon. Technol. Lett.*, vol. 29, no. 22, pp. 1943–1946, Nov. 2017.
- [4] Y. Du et al., "Detachable interface toward a low-loss reflow-compatible fiber coupling for co-packaged optics (CPO)," *Opt. Exp.*, vol. 31, 2023, pp. 1318–1329.
- [5] Z. Mathai et al., "Detachable 1x8 single mode optical interface for DWDM microring silicon photonic transceivers," *Proc. SPIE*, vol. 11286, 2020, Art. no. 112860A.
- [6] A. Israel et al., "Photonic plug for scalable silicon photonics packaging," *Proc. SPIE*, vol. 11286, 2020, Art. no. 1128607.
- [7] G. Maxwell, "Hybrid integration technology for high functionality devices in optical communications," in *Proc. Conf. Opt. Fiber Commun./Nat. Fiber Optic Engineers Conf.*, 2008, pp. 1–3.
- [8] L. Brusberg et al., "Glass platform for co-packaged optics," *IEEE J. Sel. Topics Quantum Electron.*, vol. 29, no. 3, May/Jun. 2023, Art. no. 6000210.
- [9] S. Gross et al., "Ultrafast-laser-inscribed 3D integrated photonics: Challenges and emerging applications," *Nanophotonics*, vol. 4, no. 3, pp. 332–352, 2015.
- [10] D. Choudhury et al., "Ultrafast laser inscription: Perspectives on future integrated applications," *Laser Photon. Rev.*, vol. 8, pp. 827–846, 2014, doi: [10.1002/lpor.201300195](https://doi.org/10.1002/lpor.201300195).
- [11] P. Mitchell, G. Brown, R. Thomson, N. Psaila, and A. Kar, "57 channel (19 × 3) spatial multiplexer fabricated using direct laser inscription," in *Proc. Conf. Opt. Fiber Commun.*, 2014, pp. 1–3.
- [12] N. Psaila, "3D laser direct writing for advanced photonic integration," *Proc. SPIE*, vol. 10924, 2019, Art. no. 109240U.
- [13] D. Tan et al., "Photonic circuits written by femtosecond laser in glass: Improved fabrication and recent progress in photonic devices," *Proc. SPIE*, vol. 3, Mar. 2021, Art. no. 024002, doi: [10.1117/1.AP.3.024002](https://doi.org/10.1117/1.AP.3.024002).
- [14] Y. Nasu et al., "Low-loss waveguides written with a femtosecond laser for flexible interconnection in a planar light-wave circuit," *Opt. Lett.*, vol. 30, pp. 723–725, 2005.
- [15] G. Račukaitis, "Ultra-short pulse lasers for microfabrication: A review," *IEEE J. Sel. Topics Quantum Electron.*, vol. 27, no. 6, Nov./Dec. 2021, Art. no. 1100112, doi: [10.1109/JSTQE.2021.3097009](https://doi.org/10.1109/JSTQE.2021.3097009).
- [16] ITU G.652 standard. [Online]. Available: <https://www.itu.int/rec/T-REC-G.652/recommendation.asp?lang=en&parent=T-REC-G.652-201611-I>
- [17] "Universal serial bus type C cable and connector specification," Release 2.0, Aug. 2019. [Online]. Available: <https://www.usb.org/sites/default/files/USB%20Type-C%20Spec%20R2.0%20-%20August%202019.pdf>
- [18] T. Satake et al., "Low-loss intermateability of APC-MPO connectors between different material plugs: Statistical and experimental study," in *Proc. 59th Int. Cable Connectivity Symp.*, 2010, pp. 9–17.
- [19] I. Poulopoulos et al., "Polarization-insensitive glass-to-silicon photonics coupler," *Proc. SPIE*, vol. 10924, 2019, Art. no. 1092417, doi: [10.1117/12.2510111](https://doi.org/10.1117/12.2510111).
- [20] G. Poulopoulos et al., "SiN-assisted flip-chip adiabatic coupler between SiPh and Glass OPCBs," *Proc. SPIE*, vol. 9753, 2016, Art. no. 975310, doi: [10.1117/12.2208878](https://doi.org/10.1117/12.2208878).

Nicholas Psaila (Member, IEEE) received the B.Sc. (Hons.) degree in physics from Imperial College London, London, U.K., in 2003, the M.Sc. degree in photonics and optoelectronic devices from St Andrews University, Fife, U.K., in 2004, and the Ph.D. degree in physics from Heriot Watt University, Edinburgh, U.K., in 2010. He was a Postdoctoral Research Associate with Heriot Watt University from 2009 to 2010 and then a Royal Society of Edinburgh Enterprise Fellow from 2010 to 2011. From 2011 to 2020, he was a Co-founder and CEO of Optoscribe, and then the CTO of Optoscribe until the company's acquisition by Intel in 2022. He is currently a Principal Engineer with Intel Corporation, U. K. He has authored or coauthored more than 60 journal and conference papers, holds eight patents and has more than 20 patents pending in the field of photonic devices and photonic manufacturing. His current research focuses on the development of advanced photonic technologies for use in optically interconnected computing applications. He is a member of the Optica, and holds an Associateship of the Royal College of Science.

Srikant Nekkanty received the M.S. degree in mechanical engineering and the Ph.D. degree in integrated systems engineering from The Ohio State University, Columbus, OH, USA, in 2003 and 2009, respectively. From 2009 to 2011, he was a Post-Doctoral Fellow with the Bone & Joint center, Henry Ford Hospital, Detroit, MI, USA. He joined Intel, Chandler, AZ, in 2011 and is currently a Technologist and manages the Sockets & Interconnects team, which is responsible for Intel's advanced packaging, assembly, and technology development, including co-packaged photonic applications. He holds 15 patents and more than 30 patents pending related to interconnects and semiconductor packaging technologies. He is also an Associate Editor for IEEE Transactions.

David Shia received the B.S. degree in physics and B.S. degree in aeronautics and astronautics engineering from University of Washington, Seattle, WA, USA, in 1993, the M.S. degree in aeronautics and astronautics engineering from the Massachusetts Institute of Technology, Cambridge, MA, USA, in 1995, the Ph.D. degree in applied physics from Cornell University, Ithaca, NY, USA, in 1999, and the second M.S. degree in electrical engineering from Stanford University, Stanford, CA, USA, in 2011. He is currently a Principal Engineer with Intel Corporation, Assembly and Test Technology Development Group. He holds more than 20 patents with 40 plus patents pending, spanning most of the thermomechanical areas in computer system design, semiconductor test, and electronics packaging. His research interests include co-packaged photonics and associated connector design.

Pooya Tadayon received the B.S. degree in chemistry from the University of Washington, Seattle, WA, USA, in 1993 and the Ph.D. degree in physical chemistry from Oregon State University, Corvallis, OR, USA, in 1998. From 1998 to 2018, he was a Technologist with Intel's Assembly and Test Technology Development Group. He is currently an Intel Fellow and Director of Assembly and Test Pathfinding, Intel's Ronler Acres campus, Hillsboro, OR, USA. He holds 28 patents, with more than three dozen patents pending, spanning the fields of test interconnect technology and package or product architecture. His current research focuses on advanced packaging technologies to enable 2.5/3D ICs and assembly/test solutions for co-packaged photonics that can scale to high volume.